3D Conductive Scaffolds as Neural Prostheses based on Carbon Nanotubes and Polypyrrole

Nuria Alegret,[a†,] Antonio Dominguez-Alfaro,[a,b] Jose M. González-Domínguez,[c,‡] Blanca Arnaiz,[a] Unai Cossío,[e] Susanna Bosi,[d] Ester Vázquez,[c] Pedro Ramos-Cabrer,[e,f] David Mecerreyes[b,f,*] and Maurizio Prato.[a,d,f,*]*

[a] Carbon Nanobiotechnology Group, CIC biomaGUNE, Paseo de Miramón 182, 20014 Donostia San Sebastián, Spain

[b] POLYMAT University of the Basque Country UPV/EHU, Avenida de Tolosa 72, 20018 Donostia-San Sebastián, Spain

[c] Departamento de Química Orgánica, Facultad de Ciencias y Tecnologías Químicas-IRICA, Universidad de Castilla-La Mancha, 13071 Ciudad Real, Spain

[d] Department of Chemical and Pharmaceutical Sciences, INSTM. University of Trieste, Via L. Giorgieri 1, 34127 Trieste, Italy

[e] Radioimaging and Image Analysis Platform, CIC biomaGUNE, Paseo de Miramón 182, 20014 Donostia San Sebastián, Spain

[f] Ikerasque, Basque Foundation for Science, 48013 Bilbao, Spain.

KEYWORDS. Carbon nanotubes, polypyrrole, vapour phase polymerization, conjugated polymers, 3D scaffold, tissue engineering, neural prostheses

ABSTRACT. Three-dimensional scaffolds for cellular organization need to enjoy a series of specific properties. On the one hand, the morphology, shape and porosity are critical parameters,

and eventually related with the mechanical properties. On the other hand, electrical conductivity is an important asset when dealing with electroactive cells, so it is a desirable property even if the conductivity values are not particularly high. Here, we construct 3D porous and conductive composites, where C8-D1A astrocytic cells were incubated to study their biocompatibility. The manufactured scaffolds are composed exclusively of Carbon Nanotubes (CNTs), a most promising material to interface with neuronal tissue, and polypyrrole (PPy), a conjugated polymer demonstrated to reduce gliosis, improve adaptability and increase charge-transfer efficiency in brain-machine interfaces. We developed a new and easy strategy, based on the Vapor Phase Polymerization (VPP) technique, where the monomer vapor is polymerized inside a sucrose sacrificial template containing CNT and an oxidant agent. After removing the sucrose template, a 3D porous scaffold was obtained whose physical, chemical and electrical properties were evaluated. The obtained scaffold showed very low density, high and homogeneous porosity, electrical conductivity and Young Modulus similar to the *in vivo* tissue. Its high biocompatibility was demonstrated even after 6 days of incubation, thus paving the way for the development of new conductive 3D scaffolds potentially useful in the field of electroactive tissues.

Introduction

Neurodegenerative diseases, such as Parkinson, Alzheimer or Lateral Sclerosis, are currently irreversible and finding an ultimate or partial cure to revert their consequences is one of the pending milestones of the scientific community.[1] Huge efforts are being focused on the tissue engineering research based on the "neurogenesis", a brand-new concept established in the past years according to which the neurons in the peripheral nervous system are able to regenerate also in the adult stage.[2-3] The key goal of tissue engineering is the development of stimulus-responsive biomaterials, also known as scaffolds, with easy-to-tailor properties that mimic the extracellular matrix of the native tissue. In this context, Carbon Nanotubes (CNTs) are one of the most promising materials to interface with electrically active tissues, such as the neuronal and cardiac ones. While it is well known that there is a correlation between cell membrane potential and cell proliferation,[4] it was recently demonstrated that CNTs boost the electrical activity of neurons and, furthermore, increase the number and lengths of their neurites.[5] Our group has been leading the research on the application of CNTs for nerve tissue regeneration and succeeded in the construction of 2D and 3D scaffolds for such purpose.[6] In light of our previous results it is clear that there is a need to develop a synthetic scaffold that would be biocompatible, immunologically inert, conductive, and infection-resistant to support cell outgrowth and move towards future implantation in patients.[7-14] It is worth noting that the mechanisms of regeneration of the central nervous system and cardiac tissues cannot after an injury are unclear, and some scientists assert that such regeneration is not possible. Therefore, even though traditional scaffolds for tissue engineering are desired to be biodegradable, such as in bone tissue engineering, neuronal and cardiac regeneration may require a permanent implant as a bridge between the healthy nearby cells and restore the lost functions. In these cases, a permanent implant must not be biodegradable to accomplish its purpose in the long term.

3D scaffolds are of particular relevance to mimic the three-dimensional tissue structure, and thus we would expect the cellular growth, dimension disposition and cellular connections to improve, turning the use of 3D implants in tissue engineering to restore the lost functionalities

eventually becoming a reality.[15] Such third dimension in CNT-based scaffolds could be achieved by blending with a polymeric support. The combination of CNT with numerous polymers has been extensively studied in the last years, and the materials produced showed a great potential in many different fields from biomedicine to solar cells, energy storage and electronics.[16] Polymers are used as support materials for CNTs, in the form of fibers or solid matrix allowing to play with the shape, dimensions and stiffness of the final scaffold. Ideally, the inherent ability of CNTs to favor the cellular growth could be synergically combined in a 3D scaffold with a conjugated polymeric substrate resulting in the ultimate implant for tissue regeneration of electroactive cells.

Conjugated polymers (CPs) have emerged as a novel and very promising class of electroactive biomaterial.[17] The design of electrodes based on conjugated polymers in brain-machine interface technology offers the opportunity to exploit a wide diversity of materials to reduce gliosis,[18-20] the most common brain response to chronically implanted neural electrodes. In fact, the use of conjugated polymers might result in electrodes with improved adaptability not only for the neuronal tissue, but also for other types of electroactive tissues, and increase charge-transfer efficiency. They are generally synthesized as coating of films, composites or fibers of non-conductive materials to improve their electrical properties.[21] Such versatility offers a wide range of options to modify their chemical, biological and physical properties, thus becoming very important materials for biosensors, neural prostheses, drug delivery devices and tissue engineering scaffolds.[22-23]

Polypyrrole (PPy) is among the most used and studied CPs for bio-applications,[24-25] although, as common in most CPs, its non-soluble nature in water only allows PPy to be processed as coatings or doped with stabilizing agents, such as PSS. Its conductive nature and high biocompatibility make it an outstanding material to develop scaffolds not only to be used as electrodes for recording or stimulating cell behavior, but also for an improved cell growth without any external stimulus.[18,26-27] PPy has been used to provide electrical properties to non-conductive 3D structures, by coating polymeric films onto previously synthesized non-conductive electrospun fibers, such as collagen or PLLA.[28-34] However, very little is reported about the combination of PPy and CNTs,

being most of the works related to the development of 2D films.[27, 35-38] To the best of our knowledge, a tridimensional structure purely composed of PPy and CNT has never been synthesized before.

In the present work, we succeeded in the construction of 3D porous composites formed exclusively of PPy and CNTs, and incubated astrocytic cells to evaluate its biocompatibility. We have developed a new and easy strategy, based on the well-known Vapor Phase Polymerization (VPP),[39] where pyrrole vapor is polymerized inside a template containing CNT and an oxidant agent. Astrocytes, which form part of the glia, provide support and nutrients to neurons in a healthy environment, thus have an essential function in the regeneration of neuronal tissue. Furthermore, they propagate intercellular Ca^{2+} in response to stimulation, and release transmitters,[40] thus being an ideal model to test the biocompatibility and the potential of our conductive scaffolds in neural prostheses. Our final goal is the manufacture of permanent implants, producing no harm or inflammation in the long term, able to provide the lost conductivity after, for example, brain or spinal cord injury, where a glial insulating scar might be formed, thus hindering the neuronal function and communication between the nearby healthy tissues. Therefore, we designed a non-degradable scaffold, taking advantage of the non-degradability of PPy and CNT, to act as a conductive-communicating bridge between the nearby healthy tissues. The resulting material is a very promising scaffold, with very low density, good porosity and high biocompatibility, thus paving the way for the development of new conductive 3D scaffolds by following a yet unexploited approach.

Experimental

Materials and methods

Multi-walled Carbon Nanotubes (CNTs, 99%) were purchased from Nanoamor Inc. (Stock# 1237YJS). Pyrrole (Py, 98%) was purchased from Sigma-Aldrich. Iron (III) Chloride hexahydrated ($FeCl_3 \cdot 6H_2O$) was acquired from Fisher Scientific Inc. Ethanol (synthesis grade) was pur-

chased from Carlo Erba Reagents SAS. All reagents and solvents were used as received with no further purification.

Thermogravimetric analyses were performed under air (25ml·min^{-1} flow rate) using a TGA Discovery (TA Instruments). The samples were equilibrated at 100ºC for 20 min and then heated at a rate of 10ºC·min^{-1}, in the range from 100ºC to 800ºC. Scanning Electron Microscope (SEM) measurements were performed on JEOL JSM-6490LV at 5kV, running in a point by point scanning mode. Transmission Electron Microscope (TEM) was carried out on JEOL JEM-2100F model EM-20014, which features a 200 kV Field Emission Gun (Schottky) "FEG" and an Ultra High Resolution Pole Piece "UHR". Mechanical characterization was performed with a Mecmesin MultiTest 2.5-i dynamic mechanical analyzer, using a 50N load cell and Teflon-covered steel plates as holders. The conductivity was evaluated through the electrochemical impedance spectroscopy (EIS) using frequencies in the range from 0.1 to 100.000 Hz, with an electrochemical workstation Autolab MSTAT204 Potentiostat/Galvanostat.

Micro-computed tomography (micro-CT) was used to quantify the porosity of CNT and PPy based scaffolds. High resolution micro-CT scans were performed on a SkyScan 1172 micro-CT system (Bruker micro-CT, Kontich, Belgium) at an energy and intensity level corresponding to 29 kV voltage and 175 µA current for 1200 projections. Particle analysis toolbox in ImageJ was used to determine the pore size distribution of the scaffolds. Image processing protocol has been developed to assess scaffolds' surface porosity, pore size distribution and internal canalizations.

Mouse astrocyte C8-D1A cell line was purchased from ATCC-LGC and cultured in phenol red-free DMEM media (GIBCO) completed with 2 mM L-glutamine (Gibco), 100 U·ml^{-1} penicilline, 100 µg/mL streptomycin(Gibco), 1mM sodium pyruvate and 10 % heat-inactivated fetal bovine serum (Gibco). The PBS buffer was purchased in tablets and prepared following manufacturer procedures (Sigma-Aldrich) corresponding to 10mM phosphate buffer containing 137 mM NaCl and 2.7 mM KCl at pH 7.4.

3D scaffolds synthesis and characterization

The 3D scaffolds were produced through a multi-stage process similar to the one described elsewhere.[6] 250mg of food approved sucrose was ground and passed through two mesh sieves with pore sizes of 250μm and 100μm, respectively (Fisher Scientific Inc.); the fraction collected was the one remaining in the middle of both, thus ensuring a grain size between 100μm and 250μm. CNTs (7.5mg) and the sieved sucrose (250mg) were then mixed in dry conditions and shaken overnight. Later, 10mg, 20mg or 40mg of $FeCl_3·6H_2O$ were added, corresponding to 3%, 7% and 13% of the total mass of the template, respectively, (labelled as ox-3%, ox-7% and ox-13% in the next sections) and mixed in dry conditions until obtaining a homogenous solid powder. Finally, 5μL of MilliQ water were added and the blend was mixed until a homogeneously wet material was obtained. The mixture was poured into a hollow plastic cylinder of 5mm in diameter and gently pressed from both sides to form a cylindrical-shape template. Then the template was hanged with a thread inside a schlenk flask, which was then filled with argon. Subsequently, 0.5mL of pyrrole monomer were introduced at the bottom of the schlenk flask, and the VPP was carried out varying two conditions: temperature (60ºC, 80ºC and 100ºC), and time of reaction (2h and 16h). The polymer was deposited into the interstitial cavities of the template. Once the polymerization was completed, the cylinder was immersed overnight into MilliQ water to remove the excess of oxidant and dissolve the sucrose, resulting in a cast framework made of connected empty cavities of controlled shape and dimensions. Finally, using a Soxhlet system, the scaffold was cleaned with ethanol for two days, to remove the side products and free PPy oligomers.

The synthesis and characterization of the PDMS/CNT scaffolds used as controls in this work was reported previously.[41]

Micro-computed tomography (micro-CT). Scaffolds were isolated from the background, using a thresholding procedure that was specific to this material. The values to segment the scaffold from background were optimised comparing the 2D grey scale image of a single slice with

the thresholded image. In this way, binary images were created and porosity values for each slice were assessed. Porosity values were determined as the percentage of pores' area with respect to the total area. Since the material is highly homogeneous, porosity was calculated in 10 randomly selected slices within the scaffold (n=10).

Image processing for the pore size distribution. Micro-CT images were binarized using an optimized threshold and subjected to processing steps such as dilation, erosion and watersheding. To analyze the pore distribution, the area of each pore was measured, and the equation of a circle was used to estimate an approximate value of the diameter of the pore, according to equation 1:

$$Pores = 2x(\sqrt{\frac{A_{circle}}{\pi}}) \tag{1}$$

Due to the high homogeneity of the system, the pore size distribution was calculated in n=10 2D-images randomly selected along the 3D object.

Conductivity analyses. The scaffolds were cut into cylinders of 5 x 5 mm (LxD), immersed in phosphate-buffered saline (PBS, 10mM) and degassed for 5 minutes to ensure the complete permeation of the inner porous structure. To carry out the measurements, a particular cell was designed and manufactured consisting on a sandwich of two coplanar gold electrodes and a PDMS block in between (see Figure 1 and S1). The PDMS block has a 6 mm hole in the middle to accommodate the scaffolds inside, and the same thickness as them (5 mm) to maintain its full contact with the electrodes along the experiment. The scaffolds were then placed within the PDMS container and 0.5 mL of PBS were added. The relative impedance and the charge transport behavior of PPy/CNT scaffolds were obtained by comparison with PDMS/CNT and PPy scaffolds. PDMS was fixed on the bottom Au electrode, and no leaking of the PBS solution was observed during the experiments.
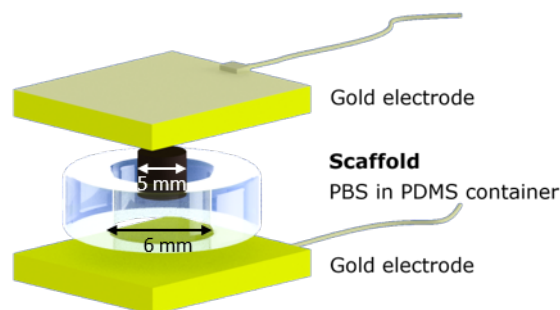
Figure 1. Schematic representation of the cell used to evaluate the tridimensional conductivity of the scaffolds developed via EIS.

Mechanical properties. Prior to mechanical testing, the scaffolds were soaked in Milli-Q water for 1-2 min and the external surplus water was carefully removed with a piece of Kimwipes®. Uniaxial compressive tests were performed under ambient conditions to the wet scaffold as it would represent a more realistic situation towards their envisioned fate, at a rate of 15 mm·min⁻¹, until reaching a 90% compressive strain. The extent of the deformation was measured by relating the measured height at each moment of the analysis with the scaffold's initial height (strain, in %). The obtained force curve was normalized to the specimens' initial diameter (stress, in kPa). Young's modulus was then obtained as the slope of the linear elastic section in the initial stages (typically from 15 to 40% strain in our case). At least 4-5 repetitions of each sample were measured.

Biocompatibility assay

Before the *in vitro* assays, the scaffolds were dipped in MilliQ water several times in order to ensure the removal of ethanol from the cleaning step. Then, they were left to dry in air and cut into thin disks of 2mm thickness. PDMS/MWCNT disks were cleaned under low-pressure oxigen plasma for 6 min (Pico Plasma Cleaner, Diener electronic) each side. Then, all the scaffolds were UV–sterilized on each side for 20 min,

Cell culture and counting. C8-D1A cells were cultured in complete media at 37 °C and 5% CO_2 in tissue culture-treated 75 cm²-flasks (Nunc). For cell passage, cells were detached from the

flasks by incubation at 37 °C with trypsin-EDTA solution 1x (2.5 g porcine trypsin and 0.2 g EDTA·4Na per liter of Hanks Balanced Salt, Sigma) and spun at 10^3 RCF for 5 min; the obtained pellet was resuspended in 1 ml of complete media and disaggregated. For cell counting, the cell suspension was serially diluted 1:10 in PBS and 1:2 in the exclusion dye Trypan Blue solution (0.4 % in 0.81 % sodium chloride and 0.06 % potassium phosphate, dibasic, Sigma). 10 µL of the diluted cell suspension was counted in a haemocytometer chamber under transmitted light in an inverted microscope (DMIL, Leica). All the 3D scaffolds were transferred to a 96-well sterile plate and incubated in 200 μL complete media for 2h at 37 °C and 5% CO_2. For cell seeding, the media was removed by aspiration and 20-50 μl complete media containing $5·10^5$ or $5·10^3$ C8-D1A cells were added carefully onto the scaffolds. The wells were filled by slowly adding 150 μL complete media and incubated for 6 or 2 days at 37 °C and 5% CO_2, respectively.

LDH assay. The viability of cells grown on the scaffolds was evaluated with the modified LDH CytoTOX96 Non-Radioactive Cytotoxicity Assay kit (Promega) reported by ali-Boucetta *et al.*[42] For cell lysis, scaffolds were transferred to a 96-well U bottom plate and mechanically disrupted by smashing after addition of 150 μL of PBS containing 9% Triton X-100 (lysis buffer, LB). Then, the samples were frozen at -80ºC for 30 min, defrosted for 20 min at 37ºC and disrupted again. The CNT-PPy-based material was separated by centrifugation at 10^3 RCF for 10min at 4ºC and supernatants were transferred to empty wells. For the LDH detection, 50 μL of each supernatant was mixed with 50 μL substrate mix and, after 4 min, the reaction was terminated by the addition of 50 μL of stop solution. Absorbance measurements at 492nm were taken in a micro plate spectrophotometer (GeniosPro, Tecan). Positive control diluted in LB 1:5000 was included as an internal control (not shown), and LB alone was used as negative control (not shown). All the collected data is represented as means of quadruplicates ±SD.

Fluorescence staining of viable cells for microscopy. Calcein-AM (Molecular Probes) staining was performed to fluorescently label live cells. The scaffolds with cells were transferred to empty wells and incubated at 37ºC for 30min with 200 μL of complete media containing 2.5 μg·ml^{-1} of Calcein-AM (Molecular Probes).

F-actin stain for cell morphology imaging. The scaffolds incubated with cells were transferred to empty wells, washed once with 200 μL PBS, fixed with 4% paraformaldehyde in PBS for 20min at 20ºC, and washed twice with PBS. Then, the cells in the scaffolds were permeabilized with 0.2% Triton X-100 in PBS for 20 min at 37ºC. For cell F-actin filament staining, the scaffolds were incubated at 37ºC for 30 min in 200 μL of media with ActinGreen488 (1:10, Molecular Probes) and washed twice with PBS before imaging.

Confocal imaging. Scaffolds with stained cells were placed in a 50mm-diammeter ≠1.5 optical glass-bottom-petri dish (Mattek) with a drop of PBS onto each scaffold disk. Images were taken in a lsm880 confocal microscope (Zeiss) employing excitation at 633nm and detection between 615-663nm in the reflection mode for scaffold imaging and excitation at 488nm with detection between 500-610nm for Calcein-AM stained cells or ActinGreen stained cells. For live imaging, the drop of PBS contained 2.5 μg·ml^{-1} Calcein-AM, and a microscope insert chamber was employed at 37ºC, 5% CO_2 and 100% humidity.

Results and discussion

Preparation of 3D conductive scaffolds by vapour phase polymerization (VPP)

Figure 2 shows a schematic representation of the manufacturing process of the conductive PPy and CNTs scaffolds. Briefly, a cylindrical template made of sieved sucrose (granularity between 100-250 μm), multi-walled pristine CNT and $FeCl_3 \cdot 6H_2O$ was hanged inside an Ar-filled schlenck. Then pyrrole monomer was introduced at the bottom and the flask was warmed-up to temperatures below to the boiling point of the monomer (131ºC). The polymerization reaction, based on the VPP method, took place inside the cylinder template, where pyrrole vapor was oxidized, polymerized and deposited within the interstitial cavities left by the sucrose template and the CNTs. Finally, in the cleaning step, the sucrose and the side-products were removed by immersion into water, first, and into ethanol, afterwards. The complete removal of Fe and Cl was confirmed by XPS analyses (see Supporting Information). As a result, a self-standing cylindrical porous template only composed of PPy and CNTs was obtained.
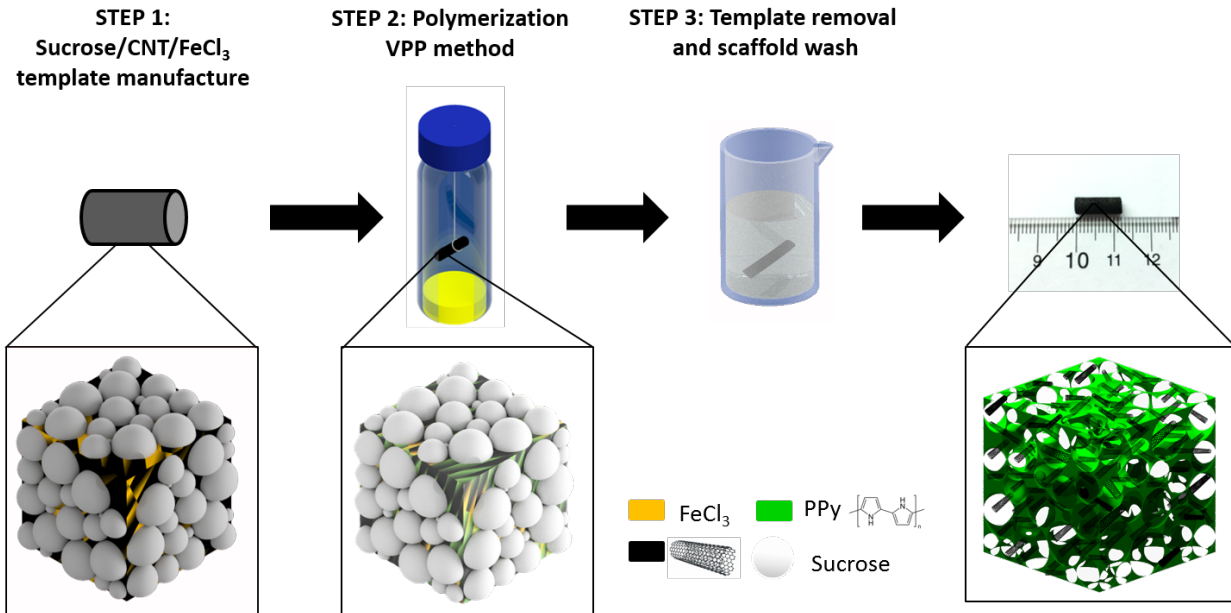
11

Figure 2. Schematic representation of the template manufacturing, polymerization and final removal of sugar and bi-products to obtain the self-standing PPy/CNT 3D scaffold.

Next, we focused our efforts in understanding how the conditions of the PPy polymerization step may affect the properties of the final scaffold. Thus, we kept constant the amount of nanotubes to reduce the experimental methodology down to three variables: (i) temperature was set at 60ºC, 80ºC or 100ºC; (ii) reaction times were of 2h or 16h and (iii) the amount of $FeCl_3 \cdot 6H_2O$ oxidant added was the 3%, 7% or 13% of the total weight of the scaffold (named from now on ox-3%, ox-7% and ox-13%, respectively). After reactions, the obtained scaffolds were characterized by thermogravimetric analysis (TGA) to elucidate the amount of polymer vs the amount of CNTs. The measurements were performed under air because these conditions allow to distinguish between polymer and CNT degradations. We have confirmed that the polymerization, thus the amount of polymer, along the whole 3D structure is homogeneous after analyzing several sections of the same scaffold with TGA; the related data is shown in the Supporting Information. Figure 3a gathers the TGA curves obtained for the scaffolds synthesized at 80 ºC, pristine CNT and the pristine polymer; the plot represents the average results obtained for three scaffolds syn-

12

thesized under the same conditions. Whereas PPy decomposes between 200ºC and 600 ºC, the CNTs only start decomposing at 500 ºC under air. Thus, 500 ºC was taken as the reference temperature to calculate the amount of PPy, considering that at such temperature the 80% of the polymer has been already decomposed while the CNTs remain almost intact (see Figure 3a). In most cases, the resulting plot indicates that the scaffold is mainly composed by CNT, in a range between 45% and 70%. The plots for the scaffolds synthesized at 60 ºC and 100 ºC are displayed in the Supporting Information.
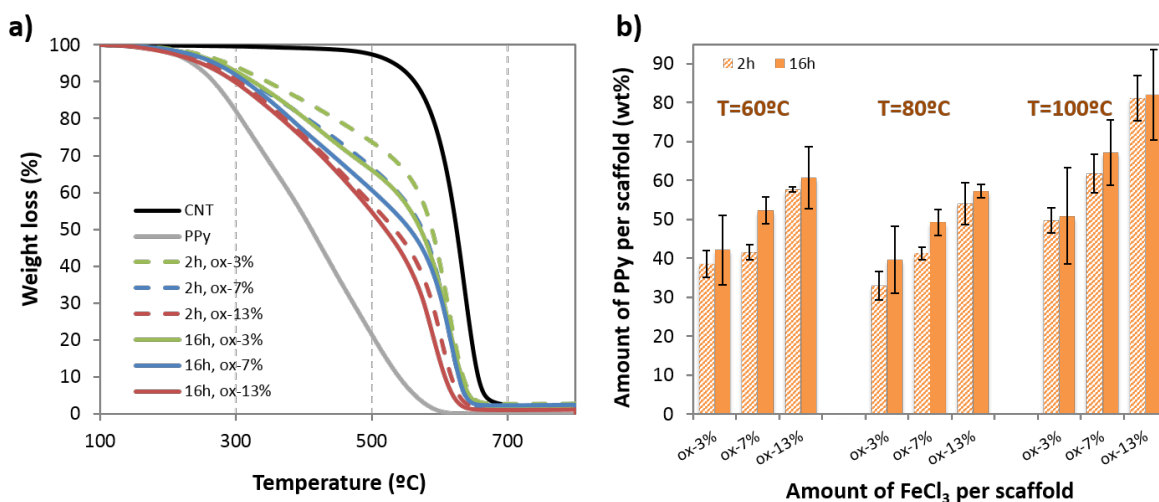
Figure 3. a) TGA plots of the polymerization performed at 80 ºC for 2h (dashed) or 16h (solid) using different amount of oxidant. b) Summary of the TGA results for the experiments performed at different temperatures (see data in the SI). Error bars indicate standard deviation after at least 3 repetitions.

Figure 3b displays the average results obtained from the variation of the three variables analyzed: temperature, time and amount of oxidant. The effect of each variable in the formation of the polymer can be summarized as follows: (i) an increase of the amount of oxidant, regardless of the polymerization time and temperature, produces an increase in the average amount of PPy obtained. In general terms, double amount of oxidant produces an increase in the amount of polymer within the scaffold between 3% and 20%, in weight. (ii) There is no significant effect of the temperature between 60ºC and 80ºC, the resulting amount of PPy synthesized is in the same

range: 30-40% of PPy for ox-3%; 41% for ox-7% and 55% for ox-13% after 2h of reaction; 40%, 50%, and 60% for ox-3%, ox-7%, and ox-13%, respectively after 16h of polymerization. On the other hand, these values increase when the polymerization is carried out at 100ºC, being the ranges of PPy around 50% for ox-3%, 65% for ox-7% and ca. 80% for ox-13%. (iii) The polymerization time is relevant at low temperatures: larger time increases the amounts of polymer synthesized, as observed for 60ºC and 80ºC (see Supporting Information). However, this effect is not observed for 100ºC, suggesting that at high temperatures the evaporation of the monomer is produced during the firsts 2h, while after that time the remaining monomer at the bottom of the flask might not be preserved in its original state and might not actively participate in the VPP process. Thus, the saturation degree of the polymerization might be achieved faster at that temperature.

In summary, different scaffolds with varying CNT/PPy ratio could be synthesized using the VPP method. We observed that such ratio is directly related to the amount of oxidant used per scaffold, the time and the temperature of the reaction. Thus, by varying the main conditions of the polymerization reaction, we are able to control the amount of polymer present in the final scaffold and, we anticipate, their properties.

Macro- and nanostructure imaging and pore size distribution

In our method, the pore size and porosity should be defined by the sucrose used as porogen or sacrificial template. Upon removal the water driven dissolution of sugar grains produced macropores inside the polymeric scaffold of irregular shapes, mimicking living tissue's irregular geometries. Pore connections were the consequence of the aggregation of sugar grains along their contact points via water driven consolidation process. The SEM pictures shown in Figure 4 reveals the porous structure of the as-synthesized 3D scaffolds at 80 ºC for 16 h using ox-7%, composed of irregularly shaped and sized pores interconnected by random paths. Interestingly, the porosity homogeneity along the whole structure can be appreciated. Similar results were ob-

tained for the scaffolds synthesized through other conditions; SEM images for other cases are presented in the Supporting Information for comparison.
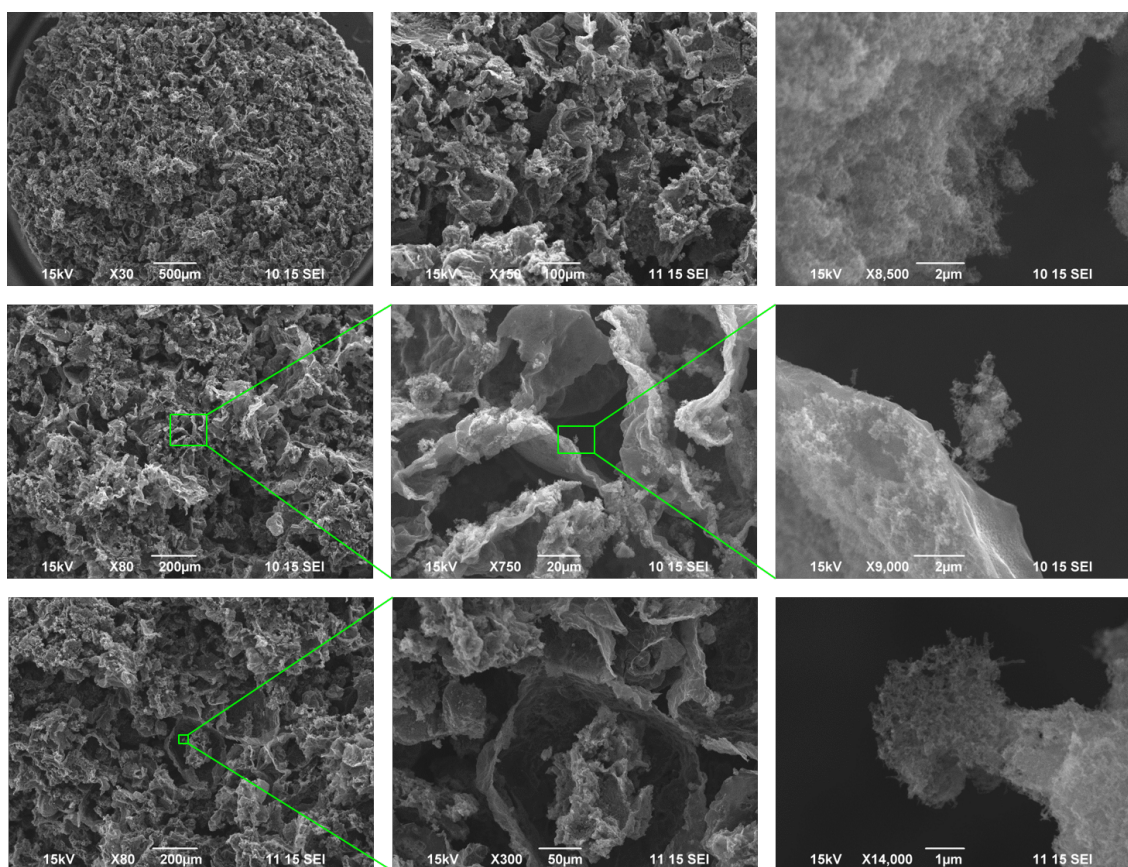

Figure 4. SEM micrographs of the 3D scaffolds (synthesized at 80ºC with ox-7% for 16h).

Pore sizes of the lowest magnification (x30) were measured using the ImageJ software. An average of seven different synthetic conditions were measured and are plotted in Figure 5. Only pores larger than 50 μm were considered. The results show that nearly half of the pores have sizes below the cut-off employed for the sucrose granularity (100 μm), which can be explained by two factors: (i) when the sucrose/CNT mixture is blended with the oxidant, most of the grains are ground into smaller particles; (ii) such pores do not come from the dissolved sucrose grains but are formed within the polymerized PPy layers. Almost 45% of the pores have the dimensions defined by the sucrose grains, ranging between 100-250 μm. Pores above 250 μm are also observed, which can be explained due to the merging of two or more sucrose grains when water is added to build the template.
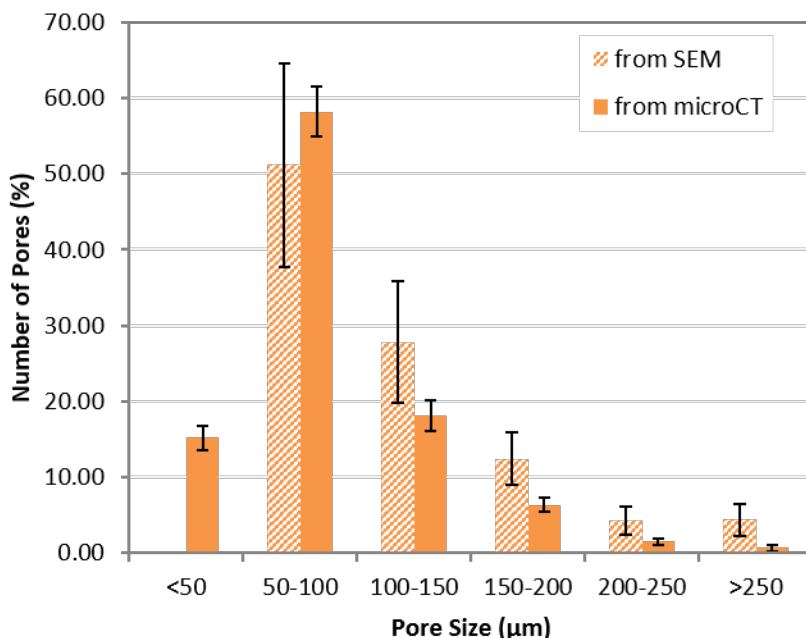
Figure 5. Pore size distribution from SEM (orange stripes) and micro-CT (solid orange) analyses.

To get a further insight into the 3D structure of the scaffolds, the same sample was analyzed by Micro-Computed Tomography (micro-CT), shown in Figure 6. The surface porosity value of these polymeric and CNT scaffolds was found to be 57.17 ± 1.16 % (n=10 slices). This means that close to 60% of the sample's area corresponds to pores and 40% to matter matching the initial sucrose loading in the scaffold. Note the small standard deviation among slices, which reflects the homogeneity of the object and supports the random selection of a finite number of 2D slices for image analysis. The analysis of micro-CT images determined macro-pore sizes between 20-300μm for PPy/CNT scaffolds. As plotted in Figure 5, almost 60% of the pores had a pore size between 50μm and 100μm. Close to 20% of the pores had a pore size between 100 μm and 150μm and 15% ranged between 20-50 μm (see Supporting Information for a higher size resolution histogram).
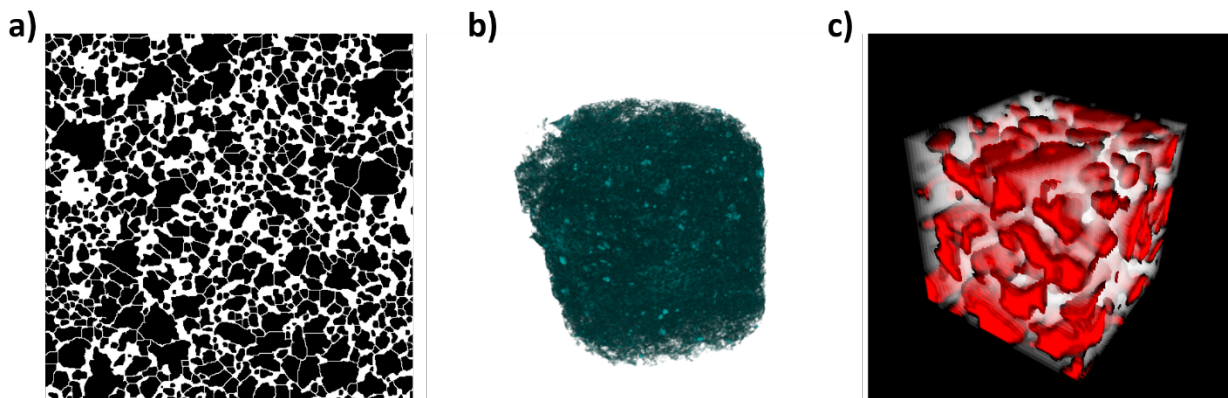
Figure 6. a) Transversal micro-CT binarised image (2D), where pores are represented in black color and matter (scaffold) in white. b) Whole scaffold's 3D volume rendered image. c) 3D illustration of scaffold's pore distribution; pores are represented in red color and matter in white.

In order to understand how PPy polymerizes inside the scaffolds and its interaction with the CNT at the nanoscale, the scaffolds were ground and dispersed in water for TEM observation. The micrographs, collected in Figure 7 (a-b), show bundles of CNT-PPy and pristine CNT along the scaffold structure. Higher magnifications reveal that only few CNT might be coated by the polymer (Figure 7c-d): most of the tubes analyzed have thicknesses within the range of the pristine CNT provided by the supplier (20-30 nm). Thicknesses up to *ca*. 46 nm were found, suggesting that the maximum thickness of the PPy-coating-CNT might be between 8-16 nm. On the other hand, the cluster pieces found in some regions (indicated with the green arrows in Figure 7 b, c and e, and dashed arrows in Figure 7d), which we assume to be bulk PPy, possibly acting as 'sticker' for the CNT, keeping the 3D structure of the whole scaffold. Such bulk appears to be composed of few or numerous polymer layers, as shown in Figure 7 f and g, respectively.
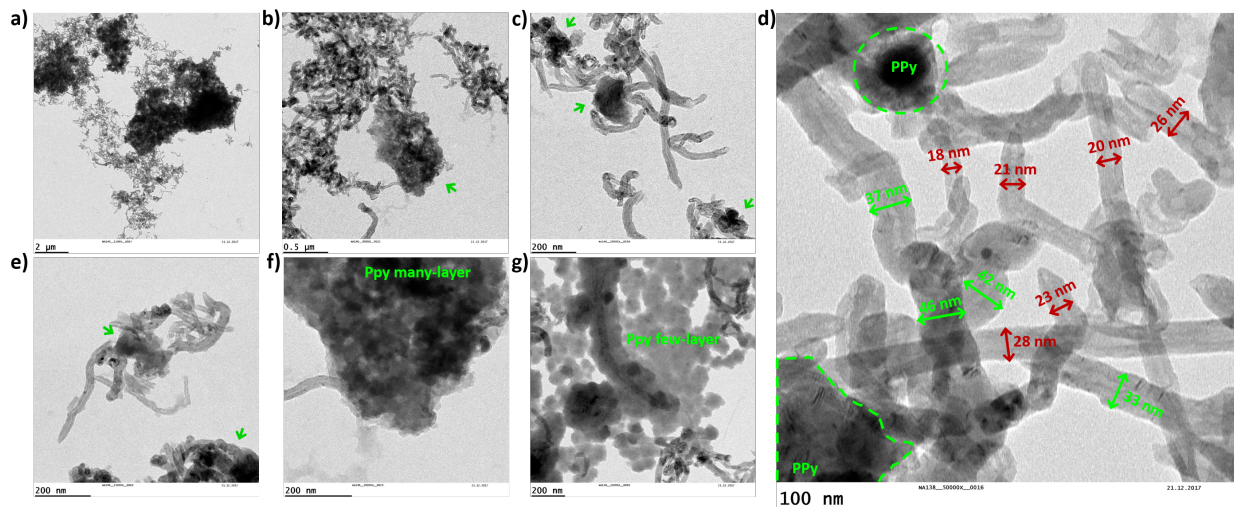
Figure 7. a-g) TEM micrographs of the CNT polymerized with PPy, from 3D scaffolds synthesized (entries 13 and 14 in Table S1). Green arrows in b), c) and e) indicate the bulk PPy 'stickers'. d) Red arrows show nanotubes with diameters within the pristine range (20-30 nm); green arrows indicate tubes with larger diameters than the pristine CNT. PPy clusters are marked with green dashed lines.

Overall, by TEM visualization we have been able to ascertain the state of dispersion and CNT-polymer interplay within our scaffolds. Instead of a continuous and uniform coating, the approach presented herein results in a random distribution of coated and uncoated CNTs, together with thick multilayered PPy clusters scattered across the structure, which we postulate that behave as brackets for CNT, thus being responsible for underpinning the structural integrity of these porous scaffolds.

Mechanical and electrical properties characterization

The mechanical properties of the scaffolds should ideally mimic the one of the body tissues. For this reason, the young modulus (YM) of our porous materials was evaluated through compression experiments of the wet scaffolds. From all the results obtained, the outliers were discarded using the interquartile method. Furthermore, the error bars were turned into confidence intervals by applying the t-Student methodology with a 95% of certainty ($\alpha = 0.05$). Figure 8

18

gathers the results obtained, relating the YM to the amount of polymer present in the scaffold. A representative cyclic compression graphs for each group is shown in Figure S7. At first glance, it is observed that the polymer increases the rigidity of the scaffold. There is a clear exponential relationship between the two variables, having larger YM for larger amounts of PPy synthesized within the scaffold. Interestingly, below 50% of PPy the increase in the YM value is not very significant, being in a range between 50kPa and 70kPa. However, from 50% on, the sample becomes noticeably more rigid, and the obtained scaffolds present values between 100kPa and 200kPa. Some of our scaffolds present similar softness to previous cross-linked hybrid hydrogels used for neuronal regeneration, which showed compressive moduli between 30 and 50 kPa.[43] These values are within the pool of typical soft porous scaffolds used for this purpose, which warrants the suitability of our scaffolds to mechanical properties requirement for neural prostheses. The brain tissue has been determined to have YM around 2 kPa, while the spinal cord has been shown to have elastic modulus around 40kPa;[44,45] thus, in the following sections, we have analyzed those scaffolds with less than 50% of PPy, which are the ones that present closer YM to the biological tissues. It is worth noting that the attempts to reduce the YM using the above-described methodology have failed since the minimum amount required of PPy to maintain the 3D structure is *ca.* 30%, which results in YM of around 50kPa.
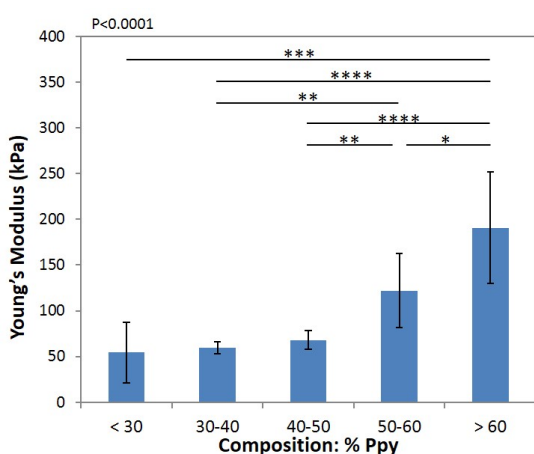

Figure 8. Young's Modulus related to the polymer composition. Statistical analyses with ANO-VA.

One of the main purposes of manufacturing PPy/CNT composites is the improvement of the conductivity. The scaffolds aimed to repair, for example, neural nerves not only must mimic the physiological environment, but also possess electrical conductivity to promote neurite outgrowth, thereby enhancing nerve regeneration.[46] Therefore, we have studied the capability of the charge transfer within a tridimensional structure using electrochemical impedance spectroscopy (EIS). Furthermore, the electrochemical impedance is an important parameter for bioapplications: implants, scaffolds or biosensors require electronic capability in contact with cells or tissue to record physiological and pathological signals or to electrically stimulate them. It is worth to remark that recently, a large number of publications have used this technique to evaluate the 3D conductivity of conductive polymeric scaffolds and it was also seen that CP lower the electrical impedance of metal electrodes.[47-51] For our purpose, PPy/CNT scaffolds, with a conductive PPy polymer matrix, were compared with PPy scaffolds without the presence of CNT and a previously reported PDMS/CNT scaffolds, with an insulating PDMS matrix.[6] All the scaffolds measured had the same cylindrical geometry and dimensions (5x5 mm, LxD) and were degassed in PBS to avoid any gas-moleucle interference during the measurements. Thus, once placed inside the designed container (see Figure 1 and methods) and filled with PBS solution, the scaffolds were in full contact with the bottom Au electrode. The device was designed with a PDMS framework of the same height as the scaffolds to ensure a full contact with the top Au electrode.

As observed in Figure 9, the impedance of PPy/CNT scaffolds ($|Z_{PPy/CNT}|$=7.8 kΩ) at 0.1 Hz was approximately four and seven times lower than that of PPy ($|Z_{PPy}|$=30 kΩ) and PDMS/CNT ($|Z_{PDMS/CNT}|$=50 kΩ), respectively, and one order of magnitude lower than the gold electrodes measured in PBS solution ($|Z_{PBS}|$=90 kΩ). We suggest that the lowest impedance of PPy/CNT comes from the formation of conducting electronic bridges between the CNT and the polymeric matrix. Furthermore, it is known the decrease impedance of the PPy layers due to the presence of electronic and ionic pathways. However, this kind of connections are not present in the PDMS/CNT scaffold, due to the non-conductive nature of PDMS, nor in the PPy scaffold, where no CNTs have been incorporated. At the same time, bode plot data (Figure 9) display a clear difference in

the maximum phase angle ~~and phase shape~~ between the scaffolds analyzed, exhibiting an increase in the maximum value of the capacitance ~~of 10~~: $\phi_{PPy/CNT}$ = -54°, ϕ_{PPy} = -67° and $\phi_{PDMS/CNT}$ = -62°. Furthermore, the phase shape of PPy and PPy/CNT scaffolds is similar, indicating their high conducting character and showing higher capacitances in the range of 10-100 Hz. Besides, in our case, the conductive nature of the PPy matrix provides an added value when dealing with neurons, being our physical characterization a landmark contribution to the field, as there is no precedent on 3D porous scaffolds made of PPy and CNT. However, there are plenty of literature data reporting electrical characterization of PPy nanocomposite films, whose conductivity was determined to be up to 600 S/cm, depending on the film thickness.[52]
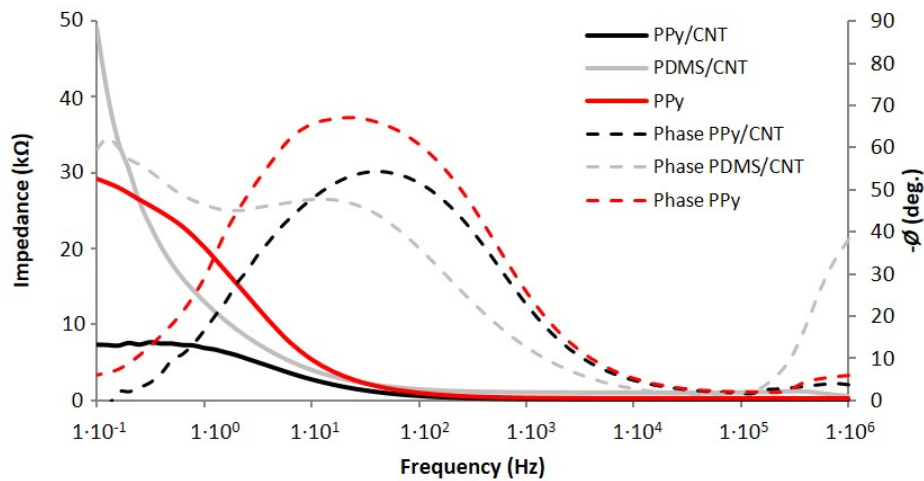

Figure 9. Impedance measurement (left axis, solid line) and phase (right axis, dashed lines) *vs* frequency plot for average PPy/CNT scaffolds (black) and PDMS/CNT scaffolds (grey).

In vitro biocompatibility of the 3D conductive scaffolds

Mouse astrocytes C8-D1A were cultured on scaffolds for 2 days and *in vitro* cytotoxicity was analyzed using a modified Lactate Dehydrogenase (LDH) assay. This method has been reported previously to circumvent all interactions between CNT and the insoluble formazan crystals formed in the commonly used 3-(4,5-Dimethylthiazol-2-yl)-2,5-Diphenyltetrazolium Bromide (MTT) or conventional LDH viability tests, and thus assessing the impact of CNT-based material

on cellular survival in a straightforward and reliable manner.[53] Cytosolic LDH is released and its activity signal was taken as a semiquantitative measurement of the number of surviving cells in the scaffolds. Once the cells are lysed, the level of absorbance of the LDH product correlates with the number of viable cells growing on the scaffolds. As all the scaffolds were seeded with the same number of astrocytes, differences would be attributed to the effect of the materials on cell survival. The previously reported PDMS/CNT was analyzed for comparison and PPy scaffolds were used as a blank control of the effect of the nanotubes on the scaffolds. Although the PDMS/CNT reported scaffold has shown similar porosity as our PPy/CNT scaffolds, we keep in mind that the differences in the mechanical properties and the hydrophilicity between the two structures come from the different nature of the polymer matrix and, unfortunately, cannot be dismissed). Figure 10a shows no difference between the absorbance of the PDMS/CNT and PPy, while the conjugation of PPy and CNT increases the absorbance significantly. Such observations not only demonstrate the non-citotoxicity of the scaffolds employed, but also that the PPy/CNT scaffolds have an enormous positive impact on the C8-D1A growth yet in the first two days of culture.
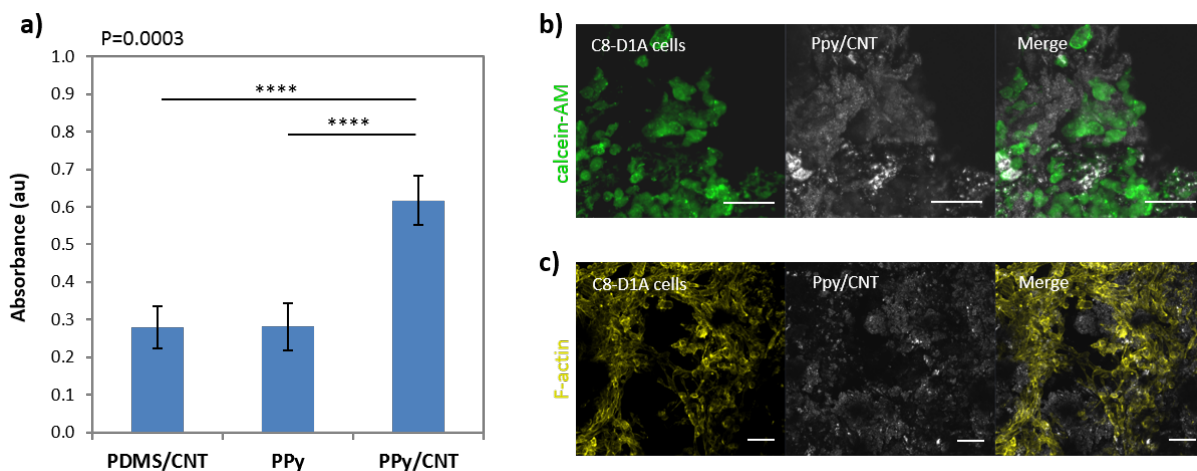

Figure 10. a) *In vitro* LDH assay of C8-D1A astrocytes cultivated for 48h on scaffolds in the presence or absence of CNTs. Absorbance readings for each scaffold are plotted as an average of 5 independent experiments (*n=4±SD*). Confocal images after b) calcein-AM stain of viable cells (green) and c) the F-actin cytoskeleton (yellow) staining of PPy/CNT scaffolds after 2 days of

culture. From left to right: stained cells (green or yellow), scaffold (grey) and merge. Images are split views of Z-stacks maximum intensity projections (57μm-optical sections). The elongated morphology of the cells indicates a good biocompatibility of the material. (Scale bar = 50μm). Statistical analysis with ANOVA.

In addition, confocal imaging was employed to analyze the cellular attachment to the PPy/CNT scaffold. Only live cells were stained with calcein-AM in fluorescent green after incubation in the scaffolds for 2 days. The 3D images in Figure 10b show high confluence of live cells adhered to the scaffold. The adhesion and proliferation of C8-D1A cells on PDMS/CNT scaffolds was also analyzed with calcein-AM staining for comparison, showing them less affinity to the PDMS-based than to the PPy-based scaffold (see Supporting Information). Furthermore, the morphology of the astrocytes was analyzed by staining their cytoskeleton with filamentous actin (F-actin, Figure 10c). Z-stacks showed certain degree of cell penetration or cell infiltration within the range of visualization allowed by the objective working distance (up to 160μm) through the pores of the scaffold (see Supplementary Information). Large elongations as well as abundant cell-to-cell contacts are clearly distinguished on the scaffold surface, suggesting the low cytotoxicity of the material, being the cells able to maintain their normal morphology and, as we anticipated, their function.

Finally, time-course viability of the astrocytes in the CNTs scaffolds was also analyzed. Briefly, 5000 C8-D1A cells were seeded on sterile PPy/CNTs or PDMS/CNTs scaffolds and cultured for 6 days. Calcein-AM staining (Figure 11) revealed an impressive growth and invasion progression for the PPy/CNT, while for the PDMS/CNT astrocyte growth was not so significant. In summary, all the abovementioned results demonstrate the outstanding ability of PPy/CNT scaffolds in astrocytic regeneration, thus suggesting its high potential as neural protheses.
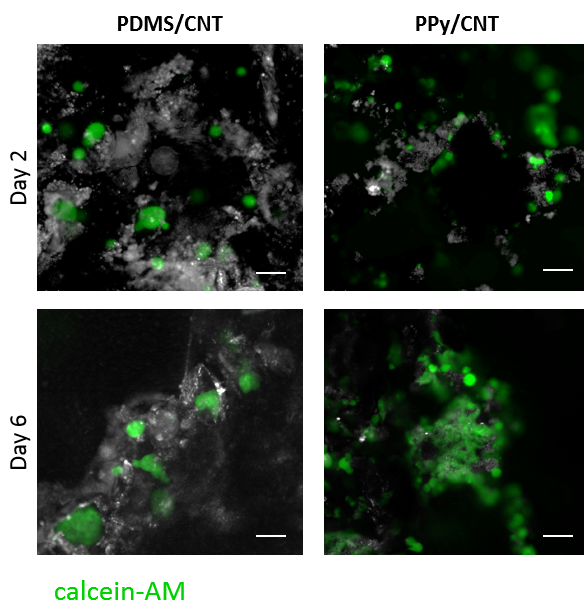
Figure 11. Confocal images after calcein-AM stain of viable cells (green) of PDMS/CNT (left) and PPy/CNT (right) scaffolds after 1 and 6 days of culture. (Scale bar = 50μm).

Conclusions

In summary, in this work we developed 3D scaffolds composed exclusively of CNTs and PPy to promote the growth of cells in the three dimensions, specifically designed with the chemical and physical properties to mimic the biological environment. This is the first time a conductive polymer is employed to build-up a self-standing 3D structure with CNT. PPy was polymerized through VPP within the macro-cavities of a previously manufactured template containing CNT; by controlling the reaction conditions we were able to adjust the desired amount of polymer introduced in the scaffold. TEM revealed how the PPy layers formed adhere to the CNT and maintain the 3D structure of the whole system. As well, it seems that some of the CNTs might be coated with a thin layer of the polymer, what would favor the underpinning effect within the entire system.

SEM and microCT analyses show the homogeneous internal structure of the final devices, mainly composed of emptiness and macro-cavities, mainly between 50-200 μm, large enough to

accommodate any kind of cell or biological entity. Besides, this porous morphology allows a significantly higher surface-to-volume ratio, resulting in low impedance, being the key feature of these manufactured devices the improved tridimensional conductivity with respect to the previously reported PDMS-based scaffolds.[6] Furthermore, mechanical properties were evaluated by compression and the resulting Young Modulus was observed to be exponentially related to the amount of polymer present and in a significant part of samples studied, the modulus approached to that of brain tissue. Finally, biocompatibility was evaluated by culturing C8-D1A astrocytes inside the scaffolds with Young Modulus similar to the biological tissue, *i.e.*, scaffolds with the lower amount of PPy. Surprisingly, yet after 48h of incubation, the PPy/CNT showed a huge stimulation effect in the cell growth, regeneration and shape, maintained after larger periods of culture. Such effect is not only caused by the presence of CNT, but also the use of a conductive polymer as a matrix of the scaffold. In conclusion, we hypothesize that the incorporation of CNT not only affects the conductivity of the 3D structures, but also may change their properties making them a completely different material.

Overall, we demonstrated that the hereby presented scaffolds fulfill all the requirements for the successful growth, development and regeneration of conductive cells. Their tridimensional structure, high conductivity, homogeneous internal structure and porosity, together with their outstanding biocompatibility and cell-growth ability, place this smart material among the most promising next-generation scaffolds for electroactive tissue prostheses. In a subsequent stage of this study, we plan to perform functional assays to validate whether there is an effect of interest to pursue this material for its final application. Thus, we will analyze further the activity and behavior of the cells, including protein secretion and gene expression, among others, and using other kind of electroactive cells, as well as the growth potential on primary cells by *in vivo* implantation of the scaffolds in injured spinal cord. We will also develop further strategies and scaffolds with lower YM for application in brain and cardiac tissues.

ASSOCIATED CONTENT

Supporting Information includes: photographs of the cell device manufactured for the conductivity measurements, XPS analyses, cyclic compression graphs, and supplementary TGA plots and data, SEM images, μCT analyses, and *in vitro* assays (Zstacks).

AUTHOR INFORMATION

Corresponding Author

* NA. E-mail: nuria.alegret@ehu.eus

* DM. E-mail: david.mecerreyes@ehu.es

* MP. E-mail: prato@units.it

Present Addresses

† Cardiovascular Institute, School of Medicine, Division of Cardiology, University of Colorado Denver Anschutz Medical Campus, 12700 E.19th Avenue, Bldg. P15, Aurora, CO, 80045, USA.

‡ Group of Carbon Nanostructures and Nanotechnology, Instituto de Carboquímica ICB-CSIC. C/ Miguel Luesma Castán 4, 50018 Zaragoza (Spain).

Author Contributions

The manuscript was written through contributions of all authors. All authors have given approval to the final version of the manuscript.

ABBREVIATIONS
VPP, Vapour Phase Polymerization; CNTs, Carbon nanotubes; PPy, Polypyrrole.

REFERENCES

1.	EU Joint Programme – Neurodegenerative Disease Research (JPND). http://www.neurodegenerationresearch.eu/about/what/ (accessed May 22nd 2018).
2.	Kandel, E. R.; Schwartz, J. H.; Jessel, T. M.; Siegelbaum, S. A.; Hudspeth, A. J., *Principles of Neural Science*. 5th ed.; McGraw Hill: Appleton and Lange, 2006.
3.	Navarro, X.; Vivó, M.; Valero-Cabré, A., Neural plasticity after peripheral nerve injury and regeneration. *Prog. Neurobiol.* **2007,** *82* (4), 163-201.
4.	Sundelacruz, S.; Levin, M.; Kaplan, D. L., Role of Membrane Potential in the Regulation of Cell Proliferation and Differentiation. *Stem Cell Rev.* **2009,** *5* (3), 231-246.
5.	Fabbro, A.; Prato, M.; Ballerini, L., Carbon Nanotubes in Neuroregeneration and Repair. *Adv. Drug Delivery Rev.* **2013,** *65* (15), 2034-2044.
6.	Bosi, S.; Rauti, R.; Laishram, J.; Turco, A.; Lonardoni, D.; Nieus, T.; Prato, M.; Scaini, D.; Ballerini, L., From 2D to 3D: Novel Nanostructured Scaffolds to Investigate Signalling in Reconstructed Neuronal Networks. *Sci. Rep.* **2015,** *5*, 9562.
7.	Gilmore, J. L.; Yi, X.; Quan, L.; Kabanov, A. V., Novel Nanomaterials for Clinical Neuroscience. *J. Neuroimmune Pharmacol.* **2008,** *3* (2), 83-94.
8.	Keefer, E. W.; Botterman, B. R.; Romero, M. I.; Rossi, A. F.; Gross, G. W., Carbon Nanotube Coating Improves Neuronal Recordings. *Nat. Nanotechnol.* **2008,** *3* (7), 434-439.
9.	Kotov, N. A.; Winter, J. O.; Clements, I. P.; Jan, E.; Timko, B. P.; Campidelli, S.; Pathak, S.; Mazzatenta, A.; Lieber, C. M.; Prato, M.; Bellamkonda, R. V.; Silva, G. A.; Kam, N. W. S.; Patolsky, F.; Ballerini, L., Nanomaterials for Neural Interfaces. *Adv. Mater.* **2009,** *21* (40), 3970-4004.
10.	Lee, W.; Parpura, V., Wiring Neurons with Carbon Nanotubes. *Front. Neuroeng.* **2009,** *2*, 8.
11.	Shein, M.; Greenbaum, A.; Gabay, T.; Sorkin, R.; David-Pur, M.; Ben-Jacob, E.; Hanein, Y., Engineered Neuronal Circuits Shaped and Interfaced with Carbon Nanotube Microelectrode Arrays. *Biomed. Microdevices* **2009,** *11* (2), 495-501.
12.	Malarkey, E. B.; Parpura, V., Carbon Nanotubes in Neuroscience. *Acta Neurochir. Suppl.* **2010,** *106*, 337-341.
13.	Fabbro, A.; Villari, A.; Laishram, J.; Scaini, D.; Toma, F. M.; Turco, A.; Prato, M.; Ballerini, L., Spinal Cord Explants Use Carbon Nanotube Interfaces To Enhance Neurite Outgrowth and To Fortify Synaptic Inputs. *ACS Nano* **2012,** *6* (3), 2041-2055.
14.	Marchesan, S.; Ballerini, L.; Prato, M., Nanomaterials for Stimulating Nerve Growth. *Science* **2017,** *356* (6342), 1010-1011.
15.	Wu, Y.; Wang, L.; Guo, B.; Shao, Y.; Ma, P. X., Electroactive Biodegradable Polyurethane Significantly Enhanced Schwann Cells Myelin Gene Expression and Neurotrophin Secretion for Peripheral Nerve Tissue Engineering. *Biomaterials* **2016,** *87*, 18-31.
16.	Martinez-Hernandez, A. L.; Velasco-Santos, C.; Castano, V. M., Carbon Nanotubes Composites: Processing, Grafting and Mechanical and Thermal Properties. *Curr. Nanosci.* **2010,** *6* (1), 12-39.
17.	Guo, B.; Ma, P. X., Conducting Polymers for Tissue Engineering. *Biomacromolecules* **2018,** *19* (6), 1764-1782.
18.	George, P. M.; Lyckman, A. W.; LaVan, D. A.; Hegde, A.; Leung, Y.; Avasare, R.; Testa, C.; Alexander, P. M.; Langer, R.; Sur, M., Fabrication and Biocompatibility of Polypyrrole Implants Suitable for Neural Prosthetics. *Biomaterials* **2005,** *26* (17), 3511-3519.

19.   Cellot, G.; Lagonegro, P.; Tarabella, G.; Scaini, D.; Fabbri, F.; Iannotta, S.; Prato, M.; Salviati, G.; Ballerini, L., PEDOT:PSS Interfaces Support the Development of Neuronal Synaptic Networks with Reduced Neuroglia Response In vitro. *Front. Neurosci.* **2015,** *9*, 521.

20.   Bauquier, S. H.; McLean, K. J.; Jiang, J. L.; Boston, R. C.; Lai, A.; Yue, Z.; Moulton, S. E.; Halliday, A. J.; Wallace, G.; Cook, M. J., Evaluation of the Biocompatibility of Polypyrrole Implanted Subdurally in GAERS. *Macromol. Biosci.* **2017,** *17* (5), 1600334.

21.   Balint, R.; Cassidy, N. J.; Cartmell, S. H., Conductive Polymers: towards a Smart Biomaterial for Tissue Engineering. *Acta Biomater.* **2014,** *10* (6), 2341-2353.

22.   Mantione, D.; Del Agua, I.; Schaafsma, W.; Diez-Garcia, J.; Castro, B.; Sardon, H.; Mecerreyes, D., Poly(3,4-ethylenedioxythiophene):GlycosAminoGlycan Aqueous Dispersions: Toward Electrically Conductive Bioactive Materials for Neural Interfaces. *Macromol. Biosci.* **2016,** *16* (8), 1227-1238.

23.   Guarino, V.; Zuppolini, S.; Borriello, A.; Ambrosio, L., Electro-Active Polymers (EAPs): A Promising Route to Design Bio-Organic/Bioinspired Platforms with on Demand Functionalities. *Polymers* **2016,** *8* (5), 185.

24.   Pelto, J.; Bjorninen, M.; Palli, A.; Talvitie, E.; Hyttinen, J.; Mannerstrom, B.; Suuronen Seppanen, R.; Kellomaki, M.; Miettinen, S.; Haimi, S., Novel Polypyrrole-Coated Polylactide Scaffolds Enhance Adipose Stem Cell Proliferation and Early Osteogenic Differentiation. *Tissue Eng. Part A.* **2013,** *19* (7-8), 882-892.

25.   Mihailescu, M.; Popescu, R. C.; Matei, A.; Acasandrei, A.; Paun, I. A.; Dinescu, M., Investigation of Osteoblast Cells Behavior in Polymeric 3D Micropatterned Scaffolds using Digital Holographic Microscopy. *Appl. Opt.* **2014,** *53* (22), 4850-4858.

26.   Lee, J. Y.; Bashur, C. A.; Goldstein, A. S.; Schmidt, C. E., Polypyrrole-coated electrospun PLGA nanofibers for neural tissue applications. *Biomaterials* **2009,** *30* (26), 4325-4335.

27.   Hernández-Ferrer, J.; Pérez-Bruzón, R. N.; Azanza, M. J.; González, M.; Moral, R.; Ansón-Casaos, A.; Fuente, J. M.; Marijuan, P. C.; Martínez, M. T., Study of Neuron Survival on Polypyrrole‐embedded Single‐walled Carbon Nanotube Substrates for Long‐term Growth Conditions. *J. Biomed. Mater. Res., Part A* **2014,** *102* (12), 4443-4454.

28.   Jin, L.; Feng, Z. Q.; Zhu, M. L.; Wang, T.; Leach, M. K.; Jiang, Q., A Novel Fluffy Conductive Polypyrrole Nano-Layer Coated PLLA Fibrous Scaffold for Nerve Tissue Engineering. *J. Biomed. Nanotechnol.* **2012,** *8* (5), 779-785.

29.   Zanjanizadeh Ezazi, N.; Shahbazi, M. A.; Shatalin, Y. V.; Nadal, E.; Mäkilä, E.; Salonen, J.; Kemell, M.; Correia, A.; Hirvonen, J.; Santos, H. A., Conductive vancomycin-loaded mesoporous silica polypyrrole-based scaffolds for bone regeneration. *Int. J. Pharm.* **2018,** *536* (1), 241-250.

30.   Xu, Q.; Jin, L.; Li, C.; Kuddannayai, S.; Zhang, Y., The Effect of Electrical Stimulation on Cortical Cells in 3D Nanofibrous Scaffolds. *RSC Adv.* **2018,** *8* (20), 11027-11035.

31.   Choi, J. S.; Park, J. S.; Kim, B.; Lee, B.-T.; Yim, J.-H., In vitro biocompatibility of vapour phase polymerised conductive scaffolds for cell lines. *Polymer* **2017,** *124*, 95-100.

32.   Björninen, M.; Gilmore, K.; Pelto, J.; Seppänen-Kaijansinkko, R.; Kellomäki, M.; Miettinen, S.; Wallace, G.; Grijpma, D.; Haimi, S., Electrically Stimulated Adipose Stem Cells on Polypyrrole-Coated Scaffolds for Smooth Muscle Tissue Engineering. *Ann. Biomed. Eng.* **2017,** *45* (4), 1015-1026.

33.   Sajesh, K. M.; Jayakumar, R.; Nair, S. V.; Chennazhi, K. P., Biocompatible conducting chitosan/polypyrrole–alginate composite scaffold for bone tissue engineering. *Int. J. Biol. Macromol.* **2013,** *62*, 465-471.

34.   Zhang, J.; Li, M.; Kang, E.-T.; Neoh, K. G., Electrical stimulation of adipose-derived mesenchymal stem cells in conductive scaffolds and the roles of voltage-gated ion channels. *Acta Biomater.* **2016,** *32*, 46-56.

35. Tu, X.; Xie, Q.; Jiang, S.; Yao, S., Electrochemical Quartz Crystal Impedance Study on the Overoxidation of Polypyrrole–Carbon Nanotubes Composite Film for Amperometric Detection of Dopamine. *Biosens. Bioelectron.* **2007,** *22* (12), 2819-2826.
36. Georgakilas, V.; Dallas, P.; Niarchos, D.; Boukos, N.; Trapalis, C., Polypyrrole/MWNT Nanocomposites Synthesized through Interfacial Polymerization. *Synth. Met.* **2009,** *159* (7-8), 632-636.
37. Liu, F.; Han, G.; Chang, Y.; Fu, D.; Li, Y.; Li, M., Fabrication of carbon nanotubes/polypyrrole/carbon nanotubes/melamine foam for supercapacitor. *J. Appl. Polym. Sci.* **2014,** *131* (2), 39779.
38. Santos, M. R. d.; Oliveira, H. P. d., Simple Method for Mass Production of Polypyrrole/Carbon Nanotubes Hybrid Artificial Muscle. *Quim. Nova* **2014**, 1000-1003.
39. Jousse, F.; Olmedo, L., Parametric Study of Vapor-Phase Polymerization of Pyrrole: An Improvement in Reproducibility. *Synth. Met.* **1991,** *41* (1), 385-388.
40. Zhou, T.; Ming, Y.; Perry, S. F.; Tatic-Lucic, S., Estimation of the physical properties of neurons and glial cells using dielectrophoresis crossover frequency. *J. Biol. Phys.* **2016,** *42* (4), 571-586.
41. Aurand, E. R.; Usmani, S.; Medelin, M.; Scaini, D.; Bosi, S.; Rosselli, F. B.; Donato, S.; Tromba, G.; Prato, M.; Ballerini, L., Nanostructures to Engineer 3D Neural-Interfaces: Directing Axonal Navigation toward Successful Bridging of Spinal Segments. *Adv. Funct. Mater.* **2018,** *28* (12), 1700550.
42. Ali-Boucetta, H.; Al-Jamal, K. T.; Müller, K. H.; Li, S.; Porter, A. E.; Eddaoudi, A.; Prato, M.; Bianco, A.; Kostarelos, K., Cellular Uptake and Cytotoxic Impact of Chemically Functionalized and Polymer-Coated Carbon Nanotubes. *Small* **2011,** *7* (22), 3230-3238.
43. Martín, C.; Merino, S.; González-Domínguez, J. M.; Rauti, R.; Ballerini, L.; Prato, M.; Vázquez, E., Graphene Improves the Biocompatibility of Polyacrylamide Hydrogels: 3D Polymeric Scaffolds for Neuronal Growth. *Sci. Rep.* **2017,** *7* (1), 10942.
44. Budday, S.; Nay, R.; de Rooij, R.; Steinmann, P.; Wyrobek, T.; Ovaert, T. C.; Kuhl, E., Mechanical Properties of Gray and White Matter Brain Tissue by Indentation. *J. Mech. Behav. Biomed. Mater.* **2015,** *46*, 318-330.
45. Karimi, A.; Shojaei, A.; Tehrani, P., Mechanical Properties of the Human Spinal Cord Under the Compressive Loading. *J. Chem. Neuroanat.* **2017,** *86*, 15-18.
46. Rivnay, J.; Inal, S.; Collins, B. A.; Sessolo, M.; Stavrinidou, E.; Strakosas, X.; Tassone, C.; Delongchamp, D. M.; Malliaras, G. G., Structural Control of Mixed Ionic and Electronic Transport in Conducting Polymers. *Nat. Commun.* **2016,** *7*, 11287.
47. Wang, S.; Guan, S.; Xu, J.; Li, W.; Ge, D.; Sun, C.; Liu, T.; Ma, X., Neural stem cell proliferation and differentiation in the conductive PEDOT-HA/Cs/Gel scaffold for neural tissue engineering. *Biomater. Sci.* **2017,** *5* (10), 2024-2034.
48. Wei, B.; Liu, J.; Ouyang, L.; Martin, D. C., POSS-ProDOT Crosslinking of PEDOT. *J. Mater. Chem. B* **2017,** *5* (25), 5019-5026.
49. Wan, A. M. D.; Inal, S.; Williams, T.; Wang, K.; Leleux, P.; Estevez, L.; Giannelis, E. P.; Fischbach, C.; Malliaras, G. G.; Gourdon, D., 3D Conducting Polymer Platforms for Electrical Control of Protein Conformation and Cellular Functions. *J. Mater. Chem. B* **2015,** *3* (25), 5040-5048.
50. Inal, S.; Hama, A.; Ferro, M.; Pitsalidis, C.; Oziat, J.; Iandolo, D.; Pappa, A. M.; Hadida, M.; Huerta, M.; Marchat, D.; Mailley, P.; Owens, R. M., Conducting Polymer Scaffolds for Hosting and Monitoring 3D Cell Culture. *Adv. Biosyst.* **2017,** *1* (6), 1700052.
51. Shi-Lei, D.; Lu, H.; Cai-Xia, D.; Xiao-Yu, W.; Lu-Hai, L.; Yen, W., 3D Printing of Aniline Tetramer-Grafted-Polyethylenimine and Pluronic F127 Composites for Electroactive Scaffolds. *Macromol. Rapid Commun.* **2017,** *38* (4), 1600551.
52. Kim, J.; Sohn, D.; Sung, Y.; Kim, E.-R., Fabrication and Characterization of Conductive Polypyrrole Thin Film Prepared by in situ Vapor-Phase Polymerization. *Synth. Met.* **2003,** *132* (3), 309-313.

53.   Ali-Boucetta, H.; Al-Jamal, K. T.; Kostarelos, K., Cytotoxic Assessment of Carbon Nanotube Interaction with Cell Cultures. In *Biomedical Nanotechnology: Methods and Protocols*, Hurst, S. J., Ed. Humana Press: Totowa, NJ, 2011; pp 299-312.

Table of Contents

PPy/CNT 3D scaffold
Conductive
3D environment
Porous

Astrocytes grow in 3D